

Hyper-X Research Vehicle Experimental Aerodynamics Test Program Overview

Scott D. Holland,* William C. Woods,† and Walter C. Engelund‡
NASA Langley Research Center, Hampton, Virginia 23681-2199

An overview is provided of the experimental aerodynamics test program to ensure mission success for the autonomous flight of the Hyper-X research vehicle, a 12-ft-long, 2700-lb lifting body technology demonstrator designed to flight demonstrate for the first time a fully airframe-integrated scramjet propulsion system. Three flights are planned, two at Mach 7 and one at Mach 10. The research vehicles will be boosted to the prescribed scramjet engine test point, where they will separate from the booster, stabilize, and initiate engine test. Following more than 5 s of powered flight and 15 s of cowl-open tares, the cowl will close, and the vehicle will fly a controlled deceleration trajectory, which includes numerous control doublets for in-flight aerodynamic parameter identification. The preflight testing activities, wind-tunnel models, test rationale, risk reduction activities, and sample results from wind-tunnel tests supporting the flight trajectory from hypersonic engine test point through subsonic flight termination are reviewed.

Nomenclature

b_{ref}	= Hyper-X vehicle reference span, ft
C_A	= axial force coefficient, (axial force/ $q_\infty S_{\text{ref}}$)
C_D	= drag force coefficient, (drag/ $q_\infty S_{\text{ref}}$)
$C_{D\delta_e}$	= drag coefficient derivative with respect to elevator deflection, deg^{-1}
C_L	= lift force coefficient, (lift/ $q_\infty S_{\text{ref}}$)
$C_{L\alpha}$	= lift coefficient derivative with respect to angle of attack, deg^{-1}
$C_{L\delta_e}$	= lift coefficient derivative with respect to elevator deflection, deg^{-1}
C_l	= rolling moment coefficient, (rolling moment/ $q_\infty S_{\text{ref}} b_{\text{ref}}$)
$C_{l\beta}$	= rolling moment coefficient derivative with respect to sideslip angle, deg^{-1}
$C_{l\delta_a}$	= rolling moment coefficient derivative with respect to aileron deflection, deg^{-1}
$C_{l\delta_r}$	= rolling moment coefficient derivative with respect to rudder deflection, deg^{-1}
C_m	= pitching moment coefficient, (pitching moment/ $q_\infty S_{\text{ref}} l_{\text{ref}}$)
$C_{m\alpha}$	= pitching moment coefficient derivative with respect to angle of attack, deg^{-1}
$C_{m\delta_e}$	= pitching moment coefficient derivative with respect to elevator deflection, deg^{-1}
C_N	= normal force coefficient, (normal force/ $q_\infty S_{\text{ref}}$)
C_n	= yawing moment coefficient, (yawing moment/ $q_\infty S_{\text{ref}} b_{\text{ref}}$)
$C_{n\beta}$	= yawing moment coefficient derivative with respect to sideslip angle, deg^{-1}
$C_{n\delta_a}$	= yawing moment coefficient derivative with respect to aileron deflection, deg^{-1}
$C_{n\delta_r}$	= yawing moment coefficient derivative with respect to rudder deflection, deg^{-1}

C_Y	= side force coefficient, (side force/ $q_\infty S_{\text{ref}}$)
$C_{Y\beta}$	= side force coefficient derivative with respect to sideslip angle, deg^{-1}
$C_{Y\delta_a}$	= side force coefficient derivative with respect to aileron deflection, deg^{-1}
$C_{Y\delta_r}$	= side force coefficient derivative with respect to rudder deflection, deg^{-1}
l_{ref}	= Hyper-X vehicle reference length, ft
q_∞	= freestream dynamic pressure ($\frac{1}{2}\rho_\infty V_\infty^2$), psf
S_{ref}	= Hyper-X vehicle reference area, ft^2
V_∞	= freestream velocity, ft/s
α	= angle of attack, deg
β	= sideslip angle, deg
δ_a	= aileron deflection angle, achieved by differential wing deflection ($\delta_{\text{rw}} - \delta_{\text{lw}}$), deg
δ_e	= elevator deflection angle, achieved by symmetric wing deflection ($\delta_{\text{rw}} + \delta_{\text{lw}}$)/2, deg
δ_{lr}	= left rudder deflection angle, deg
δ_{lw}	= left full-flying wing deflection angle, deg
δ_r	= rudder deflection angle ($\delta_{\text{lr}} + \delta_{\text{lr}}$)/2, deg
δ_{rr}	= right rudder deflection angle, deg
δ_{rw}	= right full-flying wing deflection angle, deg
ρ_∞	= freestream density, slug/ ft^3

Introduction

THE goal of the Hyper-X Program is to demonstrate and validate the technologies, the experimental techniques, and computational methods and tools for design and performance predictions of hypersonic aircraft with airframe-integrated hydrogen fueled, dual-mode combustion scramjet propulsion systems.¹ Accomplishing this goal requires flight demonstration of a hydrogen-fueled scramjet powered hypersonic aircraft. This first-of-its-kind effort is truly pioneering in that, although hypersonic propulsion systems have been studied in the laboratory environment for over 40 years, one has never before been flight tested on a complete airframe-integrated vehicle configuration. To meet budget and schedule, the flight-test vehicle design leveraged existing databases and off-the-shelf subsystem components wherever possible.²

The design evolution of the Hyper-X configuration used, as a starting point, the extensive National Aerospace Plane (NASP) database, as well as follow-on mission study programs.³ In a sense, the Hyper-X design development was the reverse of the NASP development. The NASP program failed to produce a flight vehicle due in part to insufficient technology development. The Hyper-X design development looked forward to a 200-ft operational vision vehicle⁴ but sought to design, build, and fly a minimum size flight research vehicle (because size is a major cost driver²) to demonstrate the technologies and design methodologies necessary to develop an operational global reach endoatmospheric hypersonic cruise vehicle. Such

Presented as Paper 2000-4011 at the AIAA 18th Applied Aeronautics Conference, Denver, CO, 14–17 August 2000; received 26 October 2000; revision received 23 January 2001; accepted for publication 21 June 2001. Copyright © 2001 by the American Institute of Aeronautics and Astronautics, Inc. No copyright is asserted in the United States under Title 17, U.S. Code. The U.S. Government has a royalty-free license to exercise all rights under the copyright claimed herein for Governmental purposes. All other rights are reserved by the copyright owner. Copies of this paper may be made for personal or internal use, on condition that the copier pay the \$10.00 per-copy fee to the Copyright Clearance Center, Inc., 222 Rosewood Drive, Danvers, MA 01923; include the code 0022-4650/01 \$10.00 in correspondence with the CCC.

*Assistant Branch Head, Aerothermodynamics Branch, MS 408A. Senior Member AIAA.

†Aerospace Engineer, Aerothermodynamics Branch, MS 408A. Associate Fellow AIAA.

‡Aerospace Engineer, Vehicle Analysis Branch, MS 365. Senior Member AIAA.

a vision vehicle could contribute to key national civilian and military requirements of routine, cost-effective access to space, and endo-atmospheric, rapid-response, global reach operations. Preliminary design studies performed by NASA in early fiscal year 1995 indicated that a 12-ft vehicle could be smart scaled from the 200-ft operational concept and still demonstrate scramjet powered acceleration.² Conceptual design trade studies⁵ were performed between February and May 1995, and a preliminary design was performed between March and October 1996 under phase 3 of the Dual-Fuel Airbreathing Hypersonic Vehicle Design Study contract.⁶ This preliminary design, which included basic structural design, thermal protection system selection, identification of major system/subsystem components and potential vendors, preliminary packaging, power requirements, stage separation approach, booster integration, and flight-test planning, became the government candidate vehicle for the Hyper-X program.

In July 1996, the Hyper-X program was approved by NASA Headquarters Code R (Aeronautics), and a request for proposals (RFP), based on the government candidate vehicle, was released in October 1996. The Hyper-X Launch Vehicle (HXLV) booster development contract was awarded in February 1997 and the Hyper-X Research Vehicle (HXRV) development contract was awarded in March 1997.

Prior to the release of the RFP, the experimental aerodynamics program focused on configuration screening and preliminary database development in support of control law development and preliminary trajectory evaluations (including some Monte Carlo analyses) for inclusion in the RFP. Following the contract award, the experimental aerodynamics program focused on configuration optimization/maturation and benchmarking for each phase of the flight trajectory. This paper will describe the nominal trajectory and will review the extensive wind-tunnel test program supporting the aerodatabase development⁷ along that trajectory.

Mission Profile

The nominal Hyper-X flight trajectories each begin with a boost to the scramjet engine test conditions on a modified version of a Pegasus hybrid rocket. The Hyper-X research vehicle (HXRV) is attached to the first stage of the Pegasus rocket by means of a conically shaped adapter. This mated configuration (the HXRV, the adapter, and the booster) is referred to as the Hyper-X launch vehicle (HXLV) or stack configuration and is shown in Fig. 1.

The HXLV is carried aloft under the wing of NASA's B-52, where, in the case of the first two Mach 7 experiments, it is dropped at an altitude of approximately 20,000 ft and a Mach number of 0.5. Shortly after drop, the booster solid rocket motor is ignited, and the HXLV flies a nominal ascent profile to the HXRV test point as indicated in Fig. 2. At a point just before the scramjet engine test, the Hyper-X flight vehicle is separated from the launch vehicle. The entire stage separation sequence, which occurs over a period of less than 500 ms, presents several extreme technical challenges in addition to the challenges associated with demonstrating the Hyper-X scramjet engine operation and performance. Details regarding the stage separation strategies and associated hardware simulation and testing can be found in Ref. 8. Details of the experimental test program for stage separation can be found in Ref. 9.

Immediately following the stage separation event, the HXRV control system will stabilize the vehicle, and the scramjet test portion of the experiment will begin. The scramjet engine inlet door will

be opened, and the scramjet fueling sequence will commence. A combination of silane (SiH_4) and gaseous hydrogen (H_2) is injected into the combustor region, resulting in powered scramjet engine operation. Silane is used only during the initial ignition process, after which pure hydrogen is injected and combusted. After the fuel is depleted, the flight vehicle will record several seconds of engine-off aerodynamic tare data, then the inlet cowl door will be closed, and the vehicle will perform a series of aerodynamic parameter identification maneuvers at hypersonic and supersonic flight conditions. These maneuvers will allow the basic aerodynamic stability and control characteristics of the airframe to be estimated from the flight data, which will then be compared with the preflight predictions developed using the ground-based wind-tunnel testing and analytical and computational methods. The vehicle will then fly a controlled deceleration trajectory, dissipating energy by performing a series of S turns, before flight termination at low subsonic conditions.

Model Design and Wind-Tunnel Test Philosophy

Budget and schedule considerations placed significant constraints on the wind-tunnel test activities. As the configuration matured, each latest revision had to be validated in the launch configuration, stage separation configuration, and research vehicle configuration across a range of Mach numbers. The testing program can be viewed as having three phases: screening, optimizing, and benchmarking. Early in the program when the configuration was evolving most rapidly, the program took advantage of rapid prototyping fabrication techniques to allow quick screening of several configurations, often in parallel, often for several phases of the flight, simultaneously. These early quick look models gained a schedule advantage (design and fabrication turn-around time) at a cost of limited parametrics and model fidelity. These models were designed to bracket the anticipated flight envelope to ensure that the vehicle was capable of trimmed, controlled flight at the desired test point. As the configuration matured, the program invested the additional time and resources to produce higher fidelity models with more parametrics to define the control effectiveness over a range of anticipated flight operation. The aerodatabase was continually updated as data from higher fidelity models supplanted older data. To minimize total cost, the higher fidelity models were designed for maximal flexibility with minimal part count, sized for use in multiple facilities, and constructed to be cannibalized for use in follow-on models. These trades almost always resulted in a reduction in model scale, which created challenges in obtaining parametrics sufficient to address control effectiveness and control surface interactions. Simulation results based on the data from this intermediate set of models aided in the definition of parametric requirements for a specialized set of larger-scale models designed to benchmark the control effectiveness and interactions at levels fine enough to resolve nonlinearities in the aerodynamics across the entire range of anticipated flight (complete trajectory), including off-design conditions sufficiently broad to encompass the simulation dispersions. Testing resources for these models were allocated in accordance with a three-tier program prioritization.¹⁰ The highest priority wind-tunnel data are those that are required to get the vehicle to scramjet-powered test condition. This includes the following phases (and supporting wind-tunnel test conditions): boost (Mach 0.8–10), stage separation (Mach 6 and 10, which bracket the flight-test conditions at Mach 7 and 10), and operation of the research vehicles at test conditions (Mach 6 and 10). Second priority was given to the research vehicle flight back to high subsonic speeds (from Mach 4.6 to ~ 0.8). The lowest priority was subsonic operation of the research vehicle because landing/recovery was not required as part of this program.

Figure 2 shows the flight trajectory, with model photographs superimposed on the portions of the trajectory addressed. Figure 2 will serve as a roadmap for the discussion of the experimental aerodynamics program as it relates to the HXRV. Since its inception in 1996, the extensive wind-tunnel testing program to evolve and benchmark the current configuration across all phases of the flight trajectory has utilized 15 models in 9 wind tunnels (both government and industry) with a total occupancy of more than 91 weeks. The configuration development is backed by more than 5800 wind-tunnel runs. To assess the launch vehicle aerodynamic characteristics from B-52 dispense to stage separation, tests included

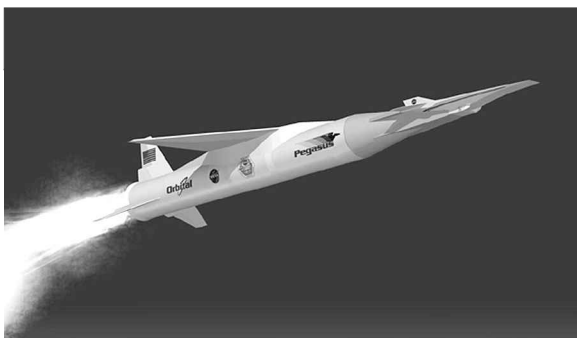


Fig. 1 HXLV configuration.

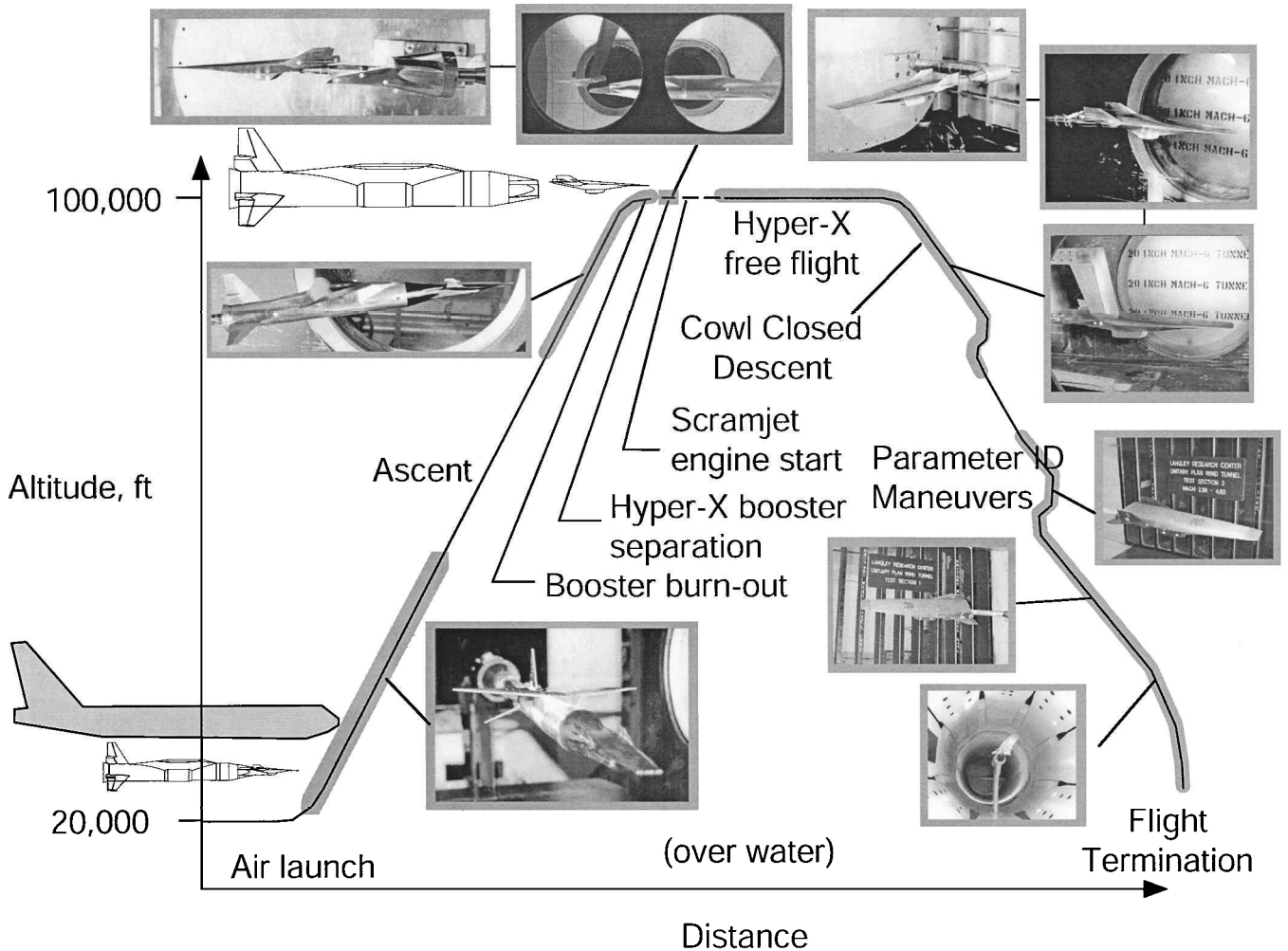


Fig. 2 Nominal Mach 7 Hyper-X flight profile superimposed with wind-tunnel test photographs.

several entries in the Lockheed Martin Vought High Speed Wind Tunnel (Grand Prairie, Texas) and several entries in NASA Langley's 16-Foot Transonic Tunnel, 20-Inch Mach 6 Air Tunnel, and 31-Inch Mach 10 Air Tunnel. (The repeated entries over the span of three years with multiple strain-gauge force and moment balances demonstrated overall measurement system stability, which, along with the within-test repeatability and estimates for wind-tunnel uncertainty, fed into the flight aerodynamics database uncertainty model.) The results from these tests and their incorporation into the launch vehicle aerodynamic database are discussed in Ref. 11. Preliminary analysis of the interference aerodynamics during the separation event was conducted using the HXRV and the adapter portion of the booster in the 20-Inch Mach 6 and 31-Inch Mach 10 Tunnels. These results led to extensive testing in the Arnold Engineering Development Center von Kármán Gas Dynamics Facility (AEDC VKF) Tunnel B at Mach 6 (Ref. 12). Six-component force and moment data were simultaneously obtained on the HXRV and booster plus adapter combination in close proximity to each other. These tests made use of the AEDC captive trajectory system rig. The details of these tests are presented in Ref. 9; a complementary computational fluid dynamic (CFD) analysis of the stage separation is provided in Ref. 13. Because of the small size of the aerodynamic force and moment models, inlet-open testing (unpowered or powered using a simulant gas technique¹⁴) was not possible. Cowl-open, fuel-on aerodynamic increments are addressed in a comprehensive CFD study,¹⁵ which has been experimentally verified at several discrete flight-test conditions by a full-scale propulsion flowpath test¹⁶ conducted in the NASA Langley Research Center 8-Foot High Temperature Tunnel. Hypersonic cowl-closed flight stability and control (both immediately before and immediately after engine test) has been the emphasis of several entries into the 20-Inch Mach 6 and 31-Inch Mach 10 Tunnels, along with a few runs piggybacked on the

stage separation test at AEDC VKF Tunnel B. Early in the program, supersonic and transonic decent aerodynamics were evaluated in the McDonnell Douglas (now Boeing) St. Louis Polysonic Wind Tunnel. As the configuration matured, these tests were superseded by tests using a larger, higher fidelity model with very fine gradations in surface control increments in the NASA Langley Research Center Unitary Plan Wind Tunnel Test Section 2 ($4.6 < \text{Mach} < 2.5$), Test Section 1 ($2.1 < \text{Mach} < 1.6$), and the 16-Foot Transonic Tunnel ($1.2 < \text{Mach} < 0.6$).

HXRV Descent Aerodynamics

It would be impossible to present in this brief overview paper the results from the entire Hyper-X experimental test program. Following a brief discussion of experimental uncertainty, this section will focus first on the aerodynamic tests performed to characterize the aerodynamics at Mach 6, in deference to the first flight, which will be at a Mach 7 engine test point. This will be followed by a summary of the across-the-speed-regime aerodynamic characteristics presented in the form of stability derivatives at selected points along the descent trajectory.

Experimental Uncertainty

An uncertainty analysis was performed based on the small-sample method of Kline and McClintock.¹⁷ Sources of uncertainty included wind-tunnel flow conditions and flow uniformity; balance calibration; model reference dimensions, areas, and contour shape; moment transfer distances; model attitude; and control surface deflection angles. Balance electrical zeros immediately before and after each run were monitored to establish balance performance during each run. Additionally, a limited number of within-test repeat runs as well as between-test repeat runs were made to allow model installation uncertainty sources to express themselves. The results of the analysis

Table 1 Experimental uncertainties (20:1 odds)

Coefficient	Uncertainty
C_N	± 0.0030
C_A	± 0.0006
C_Y	± 0.0006
C_m	± 0.0003
C_n	± 0.0003
C_l	± 0.0002
C_L	± 0.0033
C_D	± 0.0009
$C_{m\delta_e}$	± 0.0001
$C_{L\delta_e}$	± 0.0006
$C_{D\delta_e}$	± 0.0002
$C_{Y\delta_a}$	± 0.0002
$C_{n\delta_a}$	± 0.0001
$C_{l\delta_a}$	± 0.0001
$C_{Y\delta_r}$	± 0.0002
$C_{n\delta_r}$	± 0.0001
$C_{l\delta_r}$	± 0.0001
$C_{Y\beta}$	± 0.0003
$C_{n\beta}$	± 0.0001
$C_{l\beta}$	± 0.0002

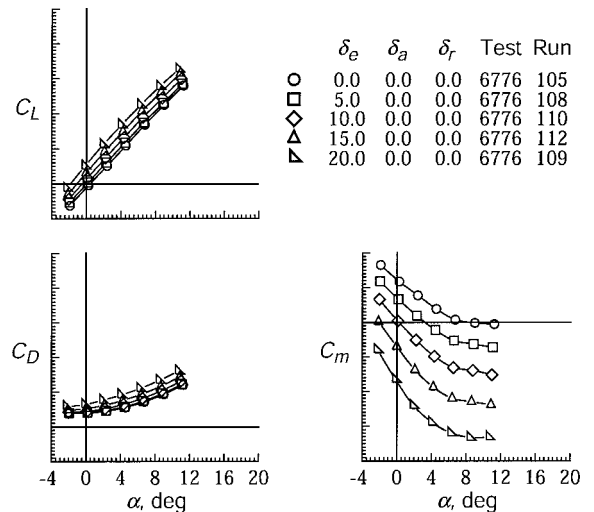
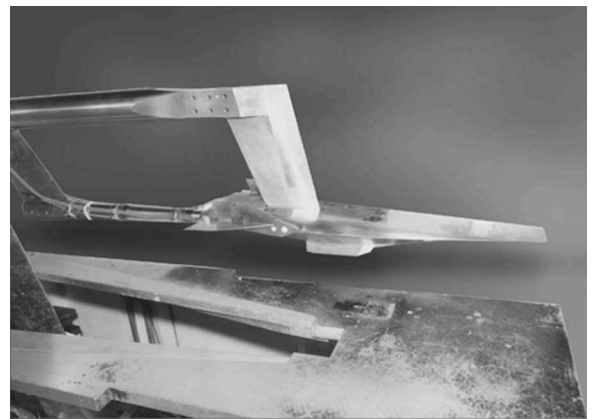
**Fig. 3 Model of KL3 HXRV at 8.33% (12-in.) scale in 20-Inch Mach 6 Tunnel.**

are presented in Table 1 for the six body-axis balance components as well as lift and drag coefficients and stability and control derivatives, at 20:1 odds. Note that error bars are omitted from the plots for clarity, in deference to Table 1.

Mach 6 HXRV Aerodynamic Characteristics

The first attempts at defining the hypersonic aerodynamics of the HXRV made use of an 8.33% (12-in.) keel line 3 (KL3) model shown in Fig. 3. In keeping with the multiuse design philosophy, this model was sized to permit a clam-shell adapter to be affixed to the sting to provide an initial assessment of the order of magnitude of the stage separation interference effects. The model parametrics included symmetric and differential horizontal tail deflections (which serve as elevator and aileron control, respectively) and rudder deflections in coarse (10-deg) increments but bracketed the expected deflection requirements. When the configuration maturation concluded, a 12.5% (18-in.) high-fidelity model (largest scale possible defined by wind-tunnel blockage concerns) was designed with parametric capabilities including horizontal tail deflections in 2.5-deg increments from -20 to $+20$ deg and rudder deflections in 5-deg increments from -20 to $+20$ deg. Also in keeping with the multiuse design philosophy, this model was designed to address support interference as part of a risk reduction activity.

The basic longitudinal aerodynamic characteristics for the HXRV airframe (inlet door closed configuration) at Mach 6 conditions are shown in Fig. 4. The experimental results, obtained on the higher fidelity 12.5% scale (18-in.) model in the most recent test entry in the NASA Langley Research Center 20-Inch Mach 6 Air Tunnel, indicate well-behaved, relatively linear lift characteristics over the anticipated flight angle of attack and elevator deflection angle range. Drag coefficient data are also shown to be well behaved with angle of attack and elevator deflection angle. The pitching moment coefficient data, shown as a function of angle of attack for elevator deflection angles between 0 and 20 deg, indicate an airframe with positive longitudinal stability (negative $C_{m\alpha}$ slope) up to angles of attack of

**Fig. 4 HXRV Mach 6 basic longitudinal aerodynamic characteristics (wind-tunnel results).****Fig. 5 Sting and blade mount adapter hardware for the HXRV wind-tunnel tests.**

approximately 8 deg. At angles of attack beyond 8 deg, the configuration becomes neutrally stable, based on the moment reference location of 46% of vehicle length (which corresponds to the design center of gravity of the flight vehicle). An elevator deflection angle of approximately 7 deg is required to trim the vehicle at the nominal flight angle of attack of 2 deg for the inlet-closed configuration.

The primary intent of the stage separation tests at AEDC was to develop the two-body interference aerodynamic models required to support the stage separation simulation activities.^{8,9} As part of that test, data on the HXRV alone (and booster alone) were also obtained. The HXRV was supported by a blade-mounted strut in the AEDC test, rather than by a conventional sting mount, so that the flowfield interference effects in the region surrounding the nozzle and base of the HXRV and the HXLV adapter were properly modeled. To account for the effects of the blade-mounted strut hardware used in the AEDC test, a separate test entry in the NASA Langley 20-Inch Mach 6 Tunnel was conducted at the same test conditions as at AEDC. As part of the NASA Langley Research Center test, a sting-mounted HXRV model was tested with a removable nonmetric dummy blade, such that the force and moment increments associated with the AEDC blade mount could be computed. A photograph of the blade and sting mount parametric model is shown in Fig. 5.

During this same test entry, the HXRV model was blade mounted and tested in the presence of a removable nonmetric dummy sting, so that a corresponding sting mount increment could be computed. An example of the results of this series of tests are shown in Fig. 6, in which the pitching moment data are shown for the HXRV configuration with the sting only, blade only, sting plus dummy blade, and blade plus dummy sting. The effect of the blade mount on pitching moment is rather dramatic. The primary influence of the presence of

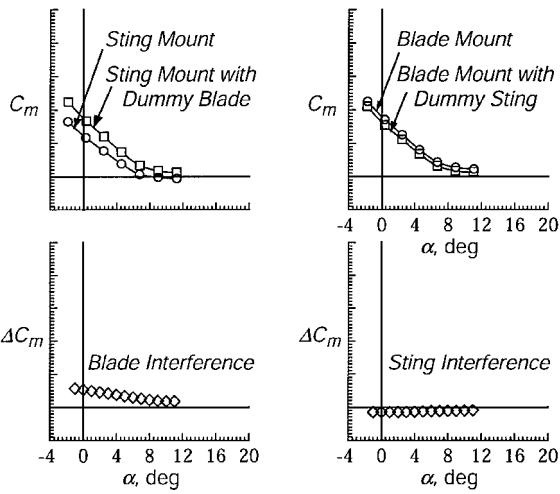


Fig. 6 Effects of the sting and blade mount interference on the HXRV Mach 6 basic longitudinal characteristics.

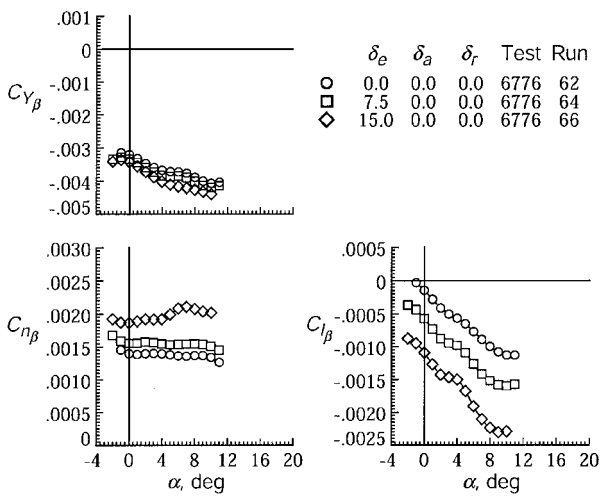


Fig. 7 Effects of elevator position on the HXRV basic lateral-directional characteristics at Mach 6.

the blade is to pressurize the upper surface aft of the center of gravity, yielding a nose-up pitching moment increment. From this series of tests, a set of blade mount increments were derived by taking the difference of the sting mount plus dummy blade results and the sting alone data. These increments were then applied to the AEDC stage separation test data to account for the blade interference effects on the forces and moments on the HXRV. A similar increment was derived from this set of test data to account for the sting mount interference; this was accomplished by taking the difference of the blade mount plus dummy sting and the blade mount alone data. The primary influence of the sting is an increase in pressure on the nozzle ramp on the lower surface, leading to a small nose-down pitching moment increment. These increments were applied to the sting mount HXRV data in the aero database.

The basic cowl-closed airframe lateral-directional characteristics from wind-tunnel tests in the NASA Langley Research Center 20-Inch Mach 6 Tunnel (Fig. 7) indicate a directionally stable vehicle (positive values of $C_{n\beta}$) over the anticipated flight angle-of-attack range. The configuration also has positive roll stability or effective dihedral (negative values of $C_{l\beta}$) and a nearly constant induced side force at sideslip conditions, $C_{Y\beta}$. The Mach 7 flight database⁷ indicates that approximately 7 deg of elevator deflection is required to trim the vehicle at 2-deg angle of attack in the inlet-closed configuration, whereas the inlet-open powered configuration trims at approximately the 0-deg elevator position. This design feature is advantageous from a vehicle performance point of view in that inlet-open power-on operation can occur with minimal trim

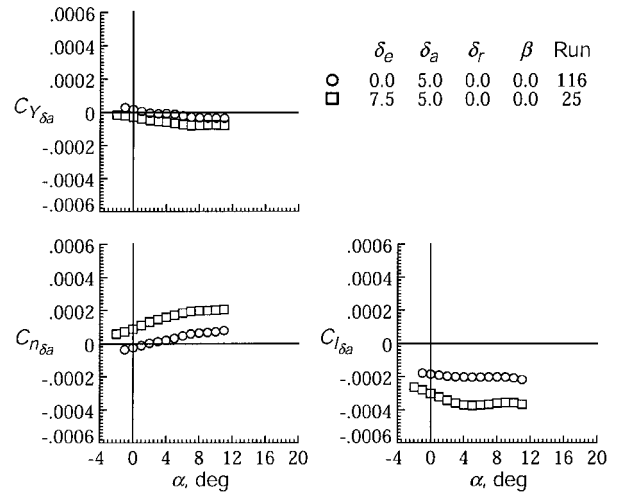


Fig. 8 Effect of elevator position on the HXRV aileron control effectiveness at Mach 6.

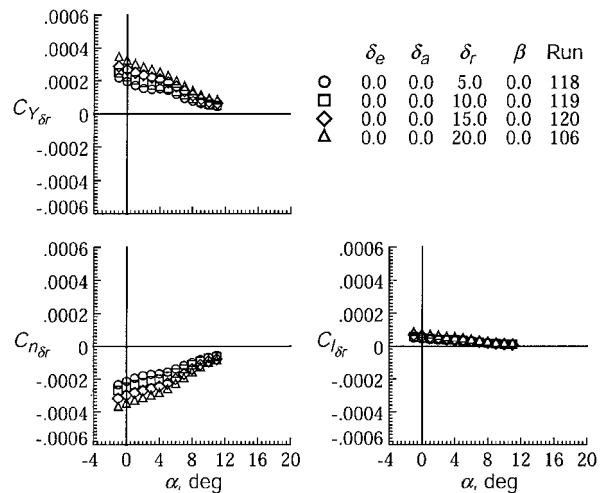


Fig. 9 Linearized Mach 6 HXRV rudder control effectiveness at 0-deg elevator position.

drag penalty. Following the engine test (cowl-closed, power-off descent), the change in trim elevator setting has an indirect effect of increasing the airframe's lateral-directional stability. At the nominal 2-deg angle-of-attack condition, there is a near 60% increase in the magnitude of the $C_{l\beta}$ term for elevator deflections of 7.5 deg vs 0 deg and a 17% increase in the $C_{n\beta}$ characteristic. Sideslip-induced side force $C_{Y\beta}$ remains moderately unaffected by elevator position.

The effect of elevator position on the aileron control power was first identified in data from the 20-Inch Mach 6 Tunnel and is shown in Fig. 8. The side force and yaw and roll moment coefficients due to linearized aileron deflections (per degree) are plotted against vehicle angle of attack. For the Hyper-X vehicle, aileron deflections are defined by asymmetric horizontal tail deflection about a nominal elevator position. For example, a +5-deg aileron deflection about a 7.5-deg elevator deflection would require a 5-deg left horizontal tail deflection and a 10-deg right horizontal tail deflection. Figure 8 indicates a strong dependence of aileron effectiveness on the nominal elevator deflection angle. In particular, the aileron roll effectiveness is almost 70% greater about a 7.5-deg elevator deflection as opposed to a 0-deg elevator deflection.

Linearized rudder derivatives, developed using measured force and moment coefficients at 5-, 10-, 15-, and 20-deg rudder deflections relative to 0-deg rudder, are provided for elevator settings of 0 and 7.5 deg in Figs. 9 and 10, respectively. Elevator effectiveness is shown to be a function not only of angle of attack, but also of the rudder deflection angle itself, increasing with increasing deflection angle. At low angles of attack, the rudders have a moderate amount of effectiveness, which appears to be only minimally affected by the

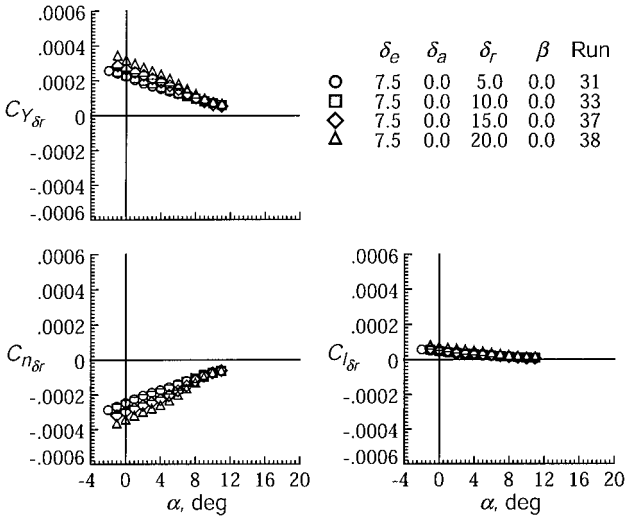


Fig. 10 Linearized Mach 6 HXRVR rudder control effectiveness at 7.5-deg elevator position.

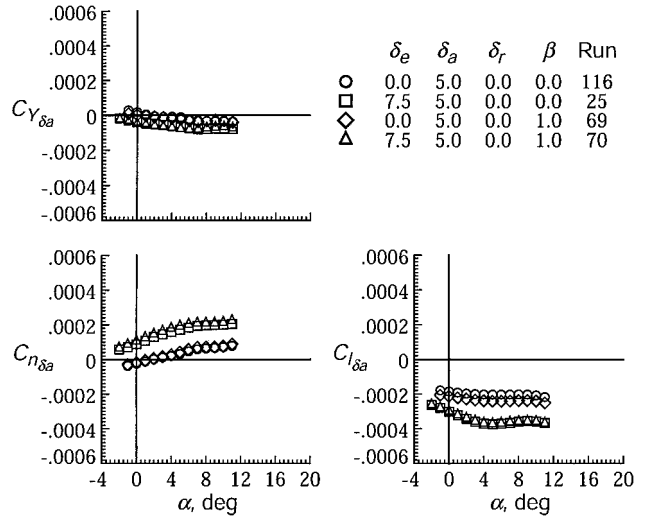


Fig. 13 Effect of sideslip on HXRVR aileron control effectiveness at Mach 6.

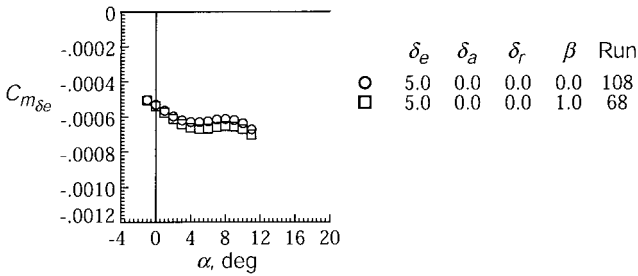


Fig. 11 Effect of sideslip on HXRVR elevator control effectiveness at Mach 6.



Fig. 14 Model of HXRVR at 20.83% (30-in.) scale in NASA Langley Research Center Unitary Plan Wind Tunnel.

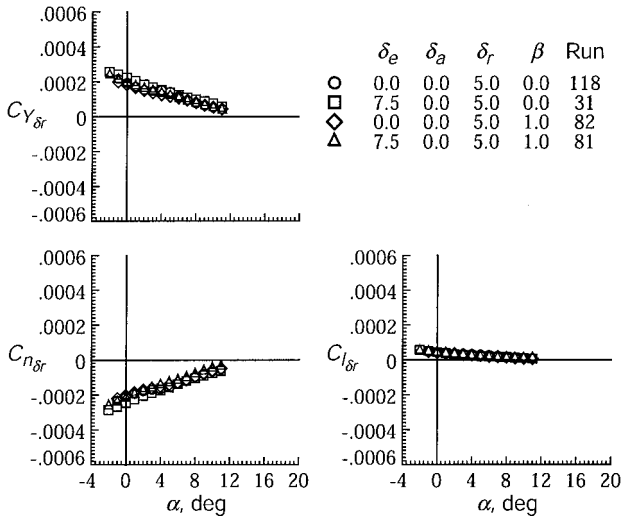


Fig. 12 Effect of sideslip on HXRVR rudder control effectiveness at Mach 6.

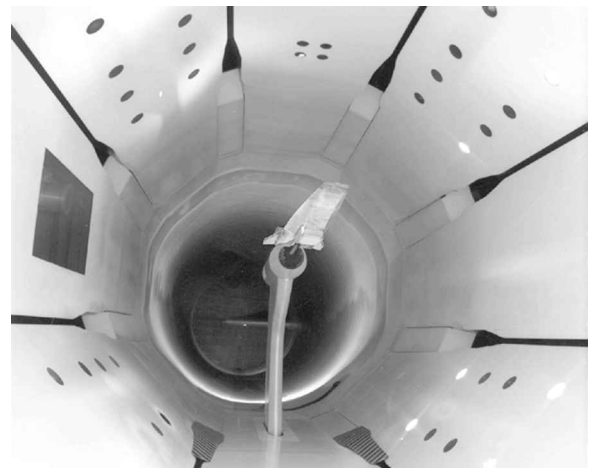


Fig. 15 Model of HXRVR at 20.83% (30-in.) scale in NASA Langley Research Center 16-Foot Transonic Wind Tunnel.

elevator position. However, as angle of attack increases, the rudders tend to lose effectiveness in a rather dramatic fashion. In fact, at angles of attack approaching 10 deg, the rudders are almost completely ineffective, as the rudders become shadowed by the forebody. The design test point is at an angle of attack of 2 deg, a condition at which the rudders do provide some degree of directional control authority. However, at a point in the flight trajectory beyond the engine test and post-test tares, the vehicle must pull up to an angle of attack of approximately 10 deg to generate enough lift to maintain its predetermined altitude profile. At this condition, the rudders will provide little in the way of directional control.

For some vehicles, control power is a function of sideslip. However, for the HXRVR, Figs. 11–13 show that the effect of sideslip on

the linearized elevator effectiveness, and rudder and aileron effectiveness at both the 0 and 7.5 deg elevator position, respectively, is minimal. As a result, the hypersonic aerodynamic database does not include sideslip sensitivity.

Supersonic/Transonic HXRVR Aerodynamics

Supersonic and transonic aerodynamic testing was performed using the 20.83% (30-in.) KL6 HXRVR model shown in Figs. 14 and 15. The model was designed to the maximum size permitted based on

expected loads and available strain gauge balances for testing in the NASA Langley Research Center Unitary Plan Wind Tunnel Test Sections 1 and 2 and the 16-Foot Transonic Tunnel. The model parameters included full-flying horizontal tail deflections (symmetric deflections for elevator, differential deflections for aileron control) in 2.5-deg increments from -20 to +20 deg and rudder deflections (symmetric deflections for rudder control, differential deflections for speed brake) in 5-deg increments from -20 to +20 deg.

Figures 16-18 present the basic longitudinal aerodynamic characteristics for the inlet-closed HXRV at elevator settings representative of trimmed conditions along the trajectory. Figure 16 presents data from Mach 4.6 down to 2.5, Fig. 17 from Mach 2.1 down to 1.6, and Fig. 18 from Mach 1.2 down to 0.6. Across the supersonic/transonic speed regime, the vehicle demonstrates positive longitudinal stability (negative $C_{m\alpha}$ slope) and well-behaved, relatively linear lift characteristics. $C_{m\alpha}$, $C_{L\alpha}$, and minimum C_D are shown to be functions of Mach number and reach their extrema at approximately Mach 1.2.

The cowl-closed lateral-directional characteristics as a function of Mach number are presented in Fig. 19. The vehicle is directionally stable (positive values of $C_{n\beta}$) across the nominal trimmed trajectory. The configuration also has positive roll stability or effective dihedral (negative values of $C_{l\beta}$), which is diminished with increasing Mach number. Figure 20 presents the aileron effectiveness as a function of Mach number. Aileron effectiveness decreases slightly with Mach

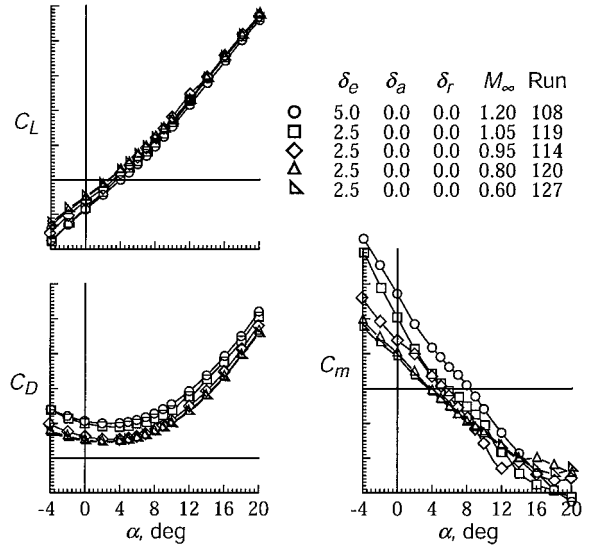


Fig. 18 Longitudinal HXRV aerodynamic characteristics from Mach 1.2 to 0.6.

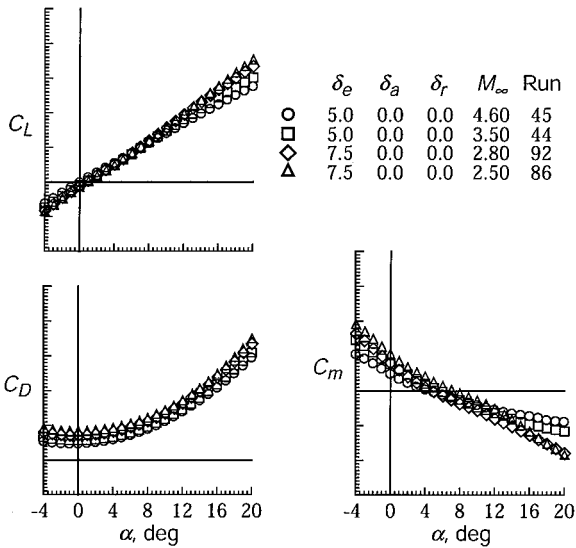


Fig. 16 Longitudinal HXRV aerodynamic characteristics from Mach 4.6 to 2.5.

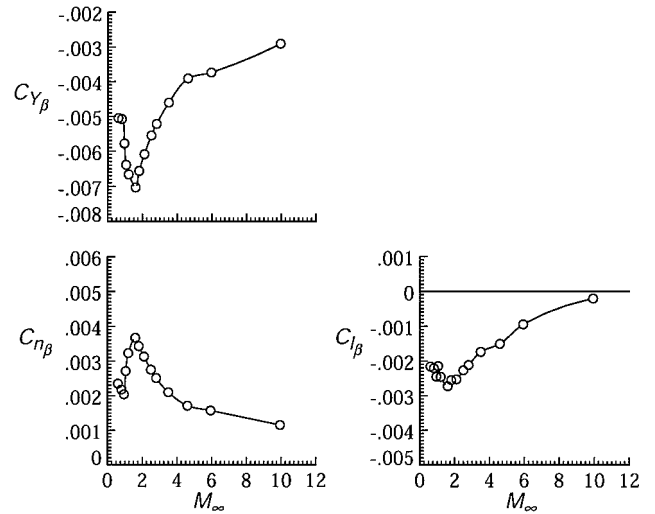


Fig. 19 Lateral-directional aerodynamic characteristics along trimmed descent trajectory.

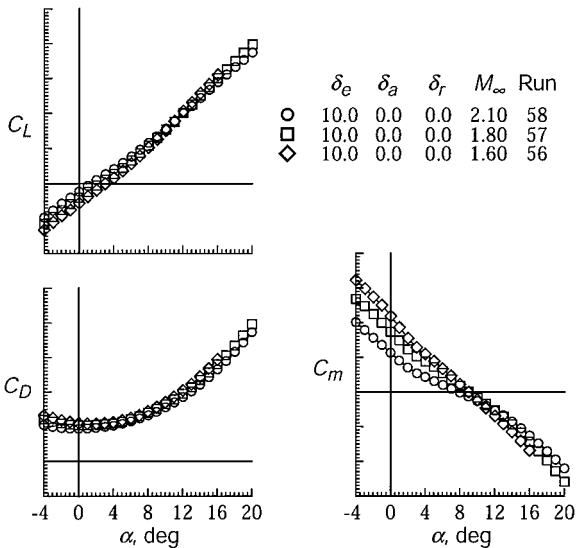


Fig. 17 Longitudinal HXRV aerodynamic characteristics from Mach 2.1 to 1.6.

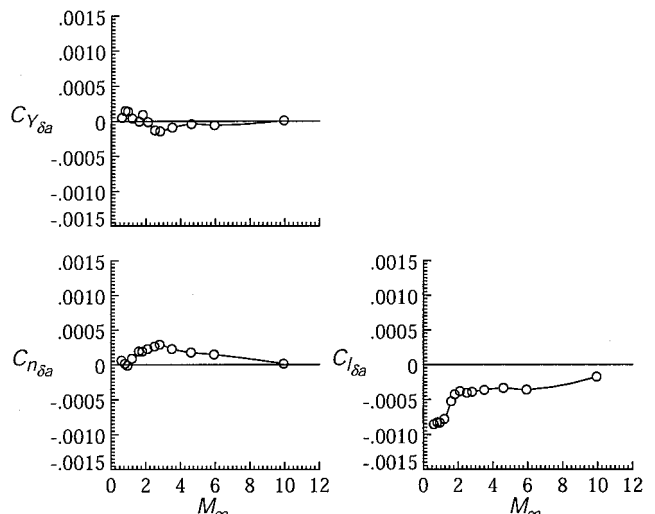


Fig. 20 Aileron effectiveness along trimmed descent trajectory.

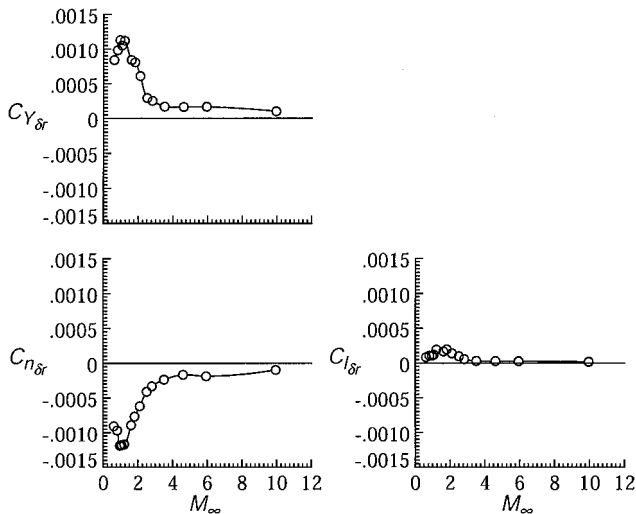


Fig. 21 Rudder effectiveness along trimmed descent trajectory.

number; Fig. 20 also shows the requirement for control coupling to null the adverse yawing moment with aileron deflection. Rudder effectiveness (Fig. 21) decreases sharply with Mach number. This is due in part to the increased angle of attack in the higher Mach number portion of the trajectory required to generate sufficient lift to maintain its predetermined altitude profile. At higher angles of attack, the rudders are shadowed by the forebody and will provide little directional control.

Conclusions

An overview has been provided of the preflight experimental aerodynamics test program for the descent trajectory of the HXRV from engine test to flight termination. Since its inception in 1996, the extensive wind-tunnel testing program to evolve and benchmark the current configuration across all phases of the flight trajectory (including transonic to hypersonic launch vehicle boost, stage separation, pre- and postengine test hypersonic flight, and controlled descent to subsonic flight termination) has utilized 15 models in 9 wind tunnels (both government and industry) with a total occupancy of more than 91 weeks. The configuration development is backed by more than 5800 wind-tunnel runs. The model design and test philosophy was reviewed. This philosophy focused on use of low-cost, rapid prototyping models with limited parametrics to provide a preliminary configuration screening, followed by optimization with higher fidelity, versatile, multiuse models, followed by precision, specialized models to provide the benchmark control aerodynamics (on- and off-design trajectory) for the flight data book. Additional risk reduction activities included extensive assessment of support interference due to both blade and sting mounting. A brief description of several of the key aerodynamic characteristics of the HXRV from scramjet operation test point to flight termination has been provided. The configuration is statically stable in three axes along the descent trajectory and has adequate control power provided by the all-moving horizontal tails and the vertical tail-rudder surfaces. The aileron control effectiveness was shown to increase substantially with elevator position at engine test point; this feature has

been included in the flight vehicle control law gain scheduling. Both the vehicle's longitudinal stability and the rudder lateral-directional control effectiveness are diminished with increased angle of attack beyond about 8 deg. The first flight of the HXRV will be performed at Mach 7. The flight trajectory includes multiple parameter identification maneuvers to determine in-flight aerodynamic performance characteristics to provide comparison with and validation of the pre-flight design and prediction methods for this first-of-its-kind, fully airframe-integrated hydrogen-fueled scramjet powered hypersonic aircraft.

References

- 1Tyson, R. W., "Hyper-X Phase I Program Plan," NASA Langley Research Center Hyper-X Program Office Document HX-419, 17 Oct. 1997.
- 2Rausch, V. L., McClinton, C. R., and Crawford, J. L., "HYPER-X: Flight Validation of Hypersonic Airbreathing Technology," International Symposium on Air Breathing Engines, ISABE Rept. 97-7024, Sept. 1997.
- 3Bogar, T. J., Alberico, J. F., Johnson, D. B., Espinosa, A. M., and Lockwood, M. K., "Dual-Fuel Lifting Body Configuration Development," AIAA Paper 96-4592, Nov. 1996.
- 4Hunt, J. L., and Eiswirth, E. A., "NASA's Dual Fuel Airbreathing Hypersonic Vehicle Study," AIAA Paper 96-4591, Nov. 1996.
- 5"Air Launched Flight Experiment Final Report," McDonnell Douglas Aerospace, St. Louis, MO, June 1995.
- 6Eiswirth, E. A., "Dual-Fuel Airbreathing Hypersonic Vehicle Design Study, Interim Report for Phase 3, Hyper-X," Rept. 98P0039, The Boeing Co., Seattle, WA, June 1998.
- 7Engelund, W. C., Holland, S. D., Cockrell, C. E., Jr., and Bittner, R. D., "Aerodynamic Database Development for the Hyper-X Airframe-Integrated Scramjet Propulsion Experiments," *Journal of Spacecraft and Rockets*, Vol. 38, No. 6, 2001, pp. 803-810.
- 8Reubush, D. E., "Hyper-X Stage Separation—Background and Status," AIAA Paper 99-4818, Nov. 1999.
- 9Woods, W. C., Holland, S. D., and DiFulvio, M., "Hyper-X Stage Separation Wind-Tunnel Test Program," *Journal of Spacecraft and Rockets*, Vol. 38, No. 6, 2001, pp. 811-819.
- 10McClinton, C. R., Holland, S. D., Rock, K. E., Engelund, W. C., Voland, R. T., Huebner, L. D., and Rogers, R. C., "Hyper-X Wind Tunnel Program," AIAA Paper 98-0553, Jan. 1998.
- 11Allen, V., "Hyper-X Launch Vehicle Aerodynamics Development," AIAA Paper 2000-4007, Aug. 2000.
- 12Collet, W. J., Davenport, A. H., and Fox, G. A., "Documentation of the NASA Hyper-X Stage Separation and Force Tests at Mach 6," Arnold Engineering Development Center, AEDC-TSR-98-P14, Arnold AFB, TN, Aug. 1998.
- 13Buning, P. G., Wong, T.-C., Dille, A. D., and Pao, J. L., "Computational Fluid Dynamics Prediction of Hyper-X Stage Separation Aerodynamics," *Journal of Spacecraft and Rockets*, Vol. 38, No. 6, 2001, pp. 820-827.
- 14Huebner, L. D., and Tatem, K. E., "CFD Code Calibration and Inlet-Fairing Effects on a 3D Hypersonic Powered-Simulation Model," AIAA Paper 93-3041, July 1993.
- 15Cockrell, C. E., Jr., Engelund, W. C., Bittner, R. D., Jentink, T. N., Dille, A. D., and Frendi, A., "Integrated Aeropropulsive Computational Fluid Dynamics Methodology for the Hyper-X Flight Experiment," *Journal of Spacecraft and Rockets*, Vol. 38, No. 6, 2001, pp. 836-843.
- 16Huebner, L. D., Rock, K. E., Witte, D. W., Ruf, E. G., and Andrews, E. H., Jr., "Hyper-X Engine Testing in the NASA Langley 8-Foot High Temperature Tunnel," AIAA Paper 2000-3605, July 2000.
- 17Kline, S. J., and McClintock, F. A., "Describing Uncertainties in Simple-Sample Experiments," *Mechanical Engineering*, Vol. 75, No. 1, 1953, pp. 3-8.

W. E. Williamson
Associate Editor